

THE INFLUENCE OF LASER POWER AND SCAN SPEED ON THE MICROSTRUCTURE, DISTORTIONS, AND MECHANICAL PROPERTIES IN THE L-PBF OF Ti-6Al-4V

G. Pollara^{1*}, D. Palmeri¹

¹Dipartimento di Ingegneria,
Università di Palermo, Viale delle Scienze, 90128 Palermo,
Italy.

*Corresponding Author's Email: gaetano.pollara@unipa.it

Article History: Received 17 May 2024; Revised 10 October 2024; Accepted 16 November 2024

©2024 G. Pollara and D. Palmeri. Published by Penerbit Universiti Teknikal Malaysia Melaka. This is an open article under the CC-BY-NC-ND license (<https://creativecommons.org/licenses/by-nc-nd/4.0/>).

ABSTRACT: Laser powder bed fusion (L-PBF) has gained a lot of interest for its ability to build complex geometries with freedom of design. The wrong choice of process parameters like laser power (P) and scan speed (v) can result in parts with low ductility, pores, and distortion. In the literature, the influence of P and v on the quality of the printed part in terms of porosity defects, distortion, and mechanical properties has been widely explored. However, to obtain functional parts without defects it is crucial to consider different aspects simultaneously. This paper aimed to fill the lack of knowledge in the literature about the combined effect of laser power and scan speed on microstructure and distortions and their influence on mechanical properties. In this frame, tensile tests, microstructural, density, and distortion measurements were carried out to study the effect of P and v on mechanical strength, ductility, density, and distortion for Ti-6Al-4V parts produced with L-PBF. Three levels of P and v were analyzed in a range of 340-380 W and 1400-1600 mm/s, respectively. From the experimental analysis, a big influence of P on the ultimate tensile strength (UTS) and density was observed. Ductility, instead, was more affected by the v. Overall, high P and v resulted in significant distortions due to the increase in thermal gradient and cooling rate. Furthermore, porosity acted as a stress-relieving factor, and as a consequence, samples with high porosity showed less distortion.

KEYWORDS: L-PBF; Ti-6Al-4V; mechanical properties; distortions.

1.0 INTRODUCTION

In recent years additive manufacturing (AM) has gained considerable interest from industries and researchers for its ability to produce components with complex shapes by adding material in a layer-by-layer construction mode, in opposition to conventional subtractive techniques [1, 2]. Among all the AM technologies, Laser Powder Bed Fusion (L-PBF) is one of the most used to produce metal parts. In this process, a powder bed is deposited on a metallic substrate, and a laser selectively melts the powder according to the slicing file. After the laser scanning, the platform is lowered, a new layer is spread, and the process is repeated until the part is completed [3]. For automotive, aerospace, and biomedical applications, Ti-6Al-4V is widely used thanks to its high mechanical properties, low density, biocompatibility, and excellent corrosion resistance [4, 5]. However, using L-PBF can result in parts with poor geometry accuracy due to thermal distortions that occur during the process [6].

The distortion of the part after removal from the substrate is a direct consequence of the residual stresses generated during the printing [7]. The origin of the residual stress can be identified in three principal factors: (i) spatial temperature gradient, (ii) thermal expansion, and (iii) plasticity and flow stress. In particular, due to localized heating and cooling by laser scanning, there is a thermal expansion/contraction of the material that leads to an instant stress redistribution to reach a new equilibrium state. The thermal stress generated during the thermal cycles can exceed the yield strength of the material and result in plastic deformations [8]. The amount of residual stresses depends on the thermal gradient and cooling rate, which, in turn, is related to the process parameters used [9]. Therefore, proper tuning of the process parameters is needed in order to minimize residual stress and distortions [10].

In the literature, there are several studies on the effect of process parameters on residual stress and distortion for Ti6Al4V components produced via L-PBF. Mugwagwa et al. [11] studied the effect of different island scanning strategies on distortion, resulting in a 40% residual stress reduction for the successive chessboard scan strategy [11]. Cheng et al. [12] also analyzed the effect of the scan strategy on residual stress and distortion, being 45°-line strategy the best solution to reduce residual stresses in both X and Y directions. The out-in scanning pattern, instead, resulted in a larger residual stress [12]. The

effect of support structure on thermal conductivity and residual stress has been evaluated by K. Zeng et al. The goal of the study was to find the minimal material used for building support structures capable of withstanding residual stress and induced part distortion [13].

T. Yu et al. highlighted the impact of the part size on the distortion of 3d printed parts. For thinner parts the distortions were larger than the ones observed for thicker parts, thus providing guidance for parts thickness design to minimize the distortion level [14]. N.C. Levkulich et al. studied the influence of different process parameters i.e., laser power, scan speed, build height, build plan area, and substrate condition on the induced residual stress during the manufacturing process. They found out that process parameters have a great influence on the rise of residual stress and distortion for L-PBF. In regard to the effect of laser power and laser speed, decreasing laser power and increasing scan speed leads to greater residual stress. In order to mitigate the overcome of residual stress it is necessary to increase the laser power or decrease the laser speed, thus increasing the melt pool cross-section. Consequently, a reduction of the cooling rate and a more uniform shrinkage of the metal is observed leading to a reduction of residual stress. Moreover, less residual stress is obtained for taller parts and with smaller build plane areas [15].

Even if the effect of process parameters on parts' distortion has been explored, it is necessary to correlate the used process parameters to the resulting mechanical processes. In fact, producing a distortion-free part is only part of the goal of the process designer; for several demanding applications, such as the ones concerning the aeronautical, aerospace, and biomedical fields, internal defects (i.e. porosities) free parts with the best possible compromise between strength and ductility must be obtained.

Z. Wang et al. first optimized laser power and scan speed values for better surface roughness and density. Then, for the range of optimal roughness and density and scan speed, they analyzed the effect of P (200–250W) and v (850–1150 mm/s) on mechanical properties. No variation of the ultimate tensile strength (UTS) was observed by varying P and v, while a clear trend was observed for the elongation to failure (ETF). Higher P resulted in low ETF, the opposite for higher v [16]. J. Lui et al. focused on finding the optimal value of P and v to obtain the maximum ductility while maintaining high tensile strength. The maximum values obtained for UTS and ETF were 1170 MPa and 10%, respectively [17].

To the authors' best knowledge, only a few papers in the literature focus on the proper choice of L-PBF process parameters taking into account their effects on both distortion and mechanical properties. J. Han et al. studied the influence of volumetric energy density (VED) on the microstructure, microhardness, residual stress, and tensile properties by varying the scanning speed and the hatch spacing. The range of 120-190 J/mm³ resulted in the optimal one to maximize density and microhardness and consequently, to obtain the maximum strength. The variation of residual stress through the specimen was evaluated qualitatively using the indentation distortion (c^2) [18]. H. Ali et al. investigated the impact of laser power and layer thickness on residual stress and mechanical properties. They found out that increasing P and decreasing exposure, while keeping a constant VED value, increased the residual stress. Lower residual stress can be obtained by increasing layer thickness, although a detrimental effect on the mechanical properties is noted [19]. In another work, the same author analyzed the effect of scan strategy on residual stress and mechanical properties.

The 90° alternating scan strategy resulted in the best solution to minimize the residual stress, while no effect on mechanical properties was observed by varying the scan strategy [20].

From the literature analysis, it is clear which strategies can be adopted to improve the quality of the L-PBF of Ti-6Al-4V. If the goal is to reduce distortion, it is possible to act on the scan strategy to have a better distribution of residual stress, using support structures to improve the thermal conductivity and reduce thermal gradient, or changing the laser power and scan speed to modify the melt-pool cross-section. Also, part geometry must be taken into account, thin walls and large build plane areas will result in large distortions. In order to improve density, the right energy amount has to be provided to the powder bed. However, even if the influence of process parameters on different aspects of the L-PBF has been studied, the relationship between part distortion, microstructure, and mechanical properties has not been deeply investigated. Understanding the mutual influence of these three aspects can help engineers in the design phase of the L-PBF of Ti-6Al-4V.

In this paper, we analyze the effect of laser power and scan speed in order to reduce distortion while maximizing density, strength, and ductility. To this end, samples were produced via L-PBF with different laser power and scan speed starting from Ti-6Al-4V powder. Each sample underwent density measurement and tensile test. The relation between distortion and mechanical properties was discussed and

proper maps were built so that the results of this study can be used by engineers in the design phase as guidance to find the best compromise between part distortion and mechanical properties for a given application.

2.0 MATERIALS AND METHODS

In this study, Ti-6Al-4V spherical powder (Figure 1a) with a size distribution of 20–63 μm was selectively laser melted using an SLM 280 HL metal 3d system provided by SLM Solutions. This machine is equipped with a 400W fiber laser [21] and works with a continuous laser emission mode where the main process parameters are the scan speed (v), laser power (P), layer thickness (t), and hatch distance (h) [22]. Dog-bone samples (Figure 1b) were produced with different values of laser power (P) and scan speed (v). In order to isolate the effect of P and v , hatch spacing (h), scan strategy (s), and layer thickness (t), were kept constant and equal to 100 μm , 0° , and 60 μm , respectively. A build orientation of 0° was chosen for the optimal density and strength of the parts.

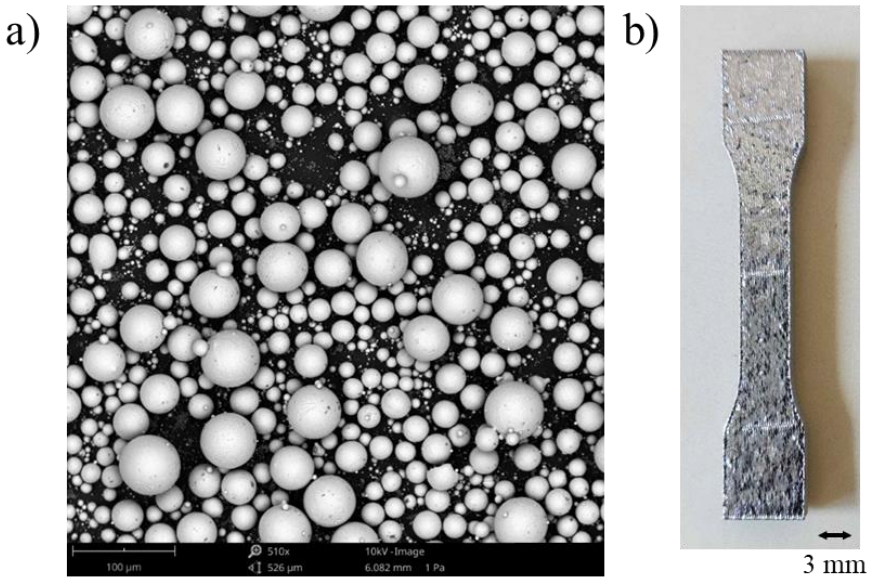


Figure 1: (a) Ti6Al4V spherical powder; (b) Dog-bone specimen used for density measurement and tensile test.

In order to study the influence of process parameters on the quality of the printed parts and understand the correlation between part

distortion, microstructure, and mechanical properties the methodology shown in Figure 2 has been followed. In the first place, process parameters were chosen by defining a grid of 3 x 3 points in the P-v plane (Figure 3) based on previous studies [7, 9] conducted by the authors. These studies have shown that at the point in the center of the parameters grid, i.e., for $P = 360 \text{ W}$ and $v = 1500 \text{ mm/s}$, the material strength in terms of UTS reaches the highest value. The grid of experimental points was also defined in order to have nearly constant Line Energy Density ($LED = P/v \text{ [J/mm]}$) values along the increasing diagonal points of the grid. Samples from ID 1 to ID 3 were fabricated by keeping a constant laser speed $v=1400 \text{ mm/s}$ and varying the laser power from $P=340 \text{ W}$ to $P=380 \text{ W}$. Samples from ID 4 to ID 6 were fabricated with a constant laser speed $v=1500 \text{ mm/s}$ and varying the laser power from 340 W to 380 W . Samples from ID 7 to ID 9 were fabricated with a constant $v=1600 \text{ mm}$ and varying the laser power from 340 W to 380 W .

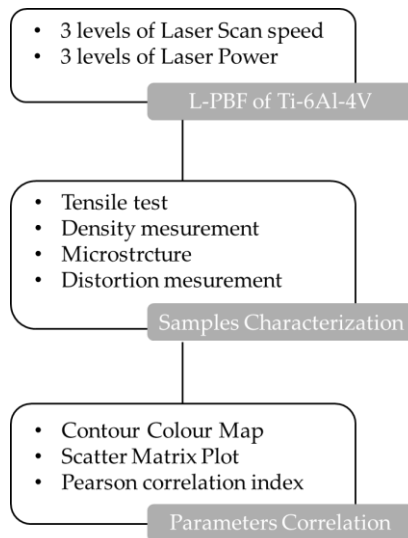


Figure 2. Research flow diagram

To evaluate the effect of process parameters on the mechanical properties, samples underwent tensile tests. To this aim, for each combination of P and v , three dog-bone specimens were designed as a reduction of the Standard ASTM/E8 with a gauge cross-section of $3\text{mm} \times 5\text{mm}$ and a gauge length of 18 mm were fabricated (Figure 1b). The samples were tested using a Galdabini Sun 5 universal testing machine at a constant rate of 1mm/s . Each sample was also weighted in air and in water to calculate the relative density (ρ_R) of the material through

Archimedes' principle. A benchmark density value of 4,43 g/cm³ was used for Ti-6Al-4V. For this purpose, a Kern EMB-V balance with a 0.001 g accuracy was used.

In order to analyze the impact of laser power and scanning speed on part distortion, the geometry of the sample, after the removal from the plate, was acquired thanks to a 3D COMET V.

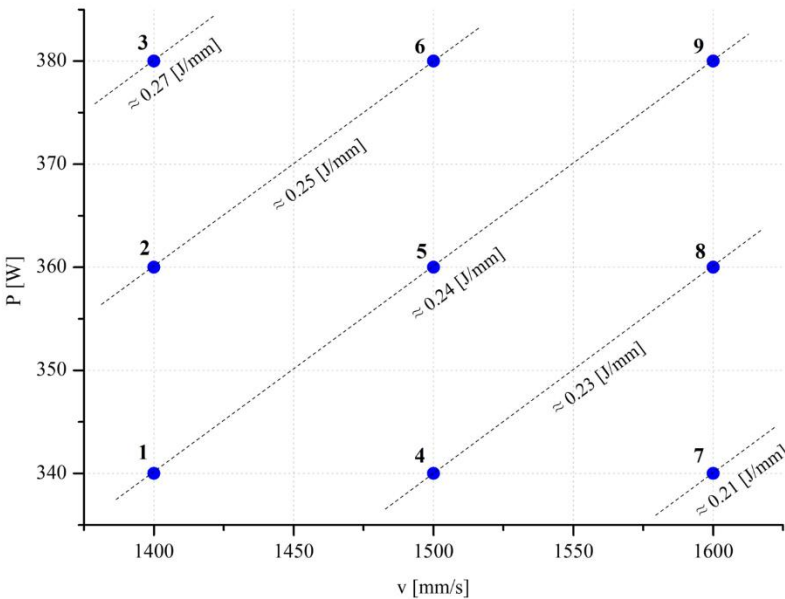


Figure 3: Grid of 3 x 3 experimental points in the P-v plane with test IDs and dotted lines with constant Line Energy Density.

This 3D acquisition system is based on the fringe projection technique where a structured light pattern is projected onto the object surface with a projection unit. The image of the fringe pattern is phase-modulated by the object's geometric features, and it is recorded by the image acquisition unit. Through the use of a processing/analysis unit, it is possible to obtain a point cloud image that can be converted to an STL file. This acquisition system allows high-resolution 3D reconstruction in a non-contact approach [23].

The acquired geometry was then compared to the original CAD model of the printed part in order to quantitatively evaluate the distortion of

the part after the process (Figure 4). Each sample was also subjected to metallographic characterization by appropriate grinding and polishing phases, followed by etching with Kroll's reagent to highlight the microstructure of the material. Metallographic images were acquired for each sample at 100X magnification using a metallographic optical microscope (Figure 5). The acquired micrographs, appropriately calibrated, made it possible to determine the average size of the original β grain, within which, during the printing process and as a result of the rapid cooling of the alloy, the metastable martensitic phase α' originates.

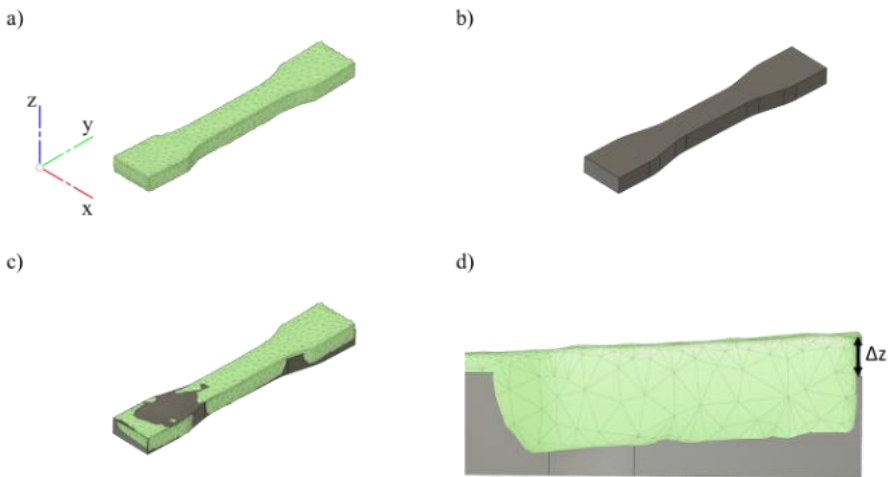


Figure 4: Quantitative evaluation of distortions: (a) acquired printed geometry; (b) CAD model; (c) overlapping between the CAD model and the acquired printed geometry; (d) evaluation of distortions in the z-build direction.

The average grain size was calculated using the intercept technique based on the use of the micrographs acquired at 100X magnification.



Figure 5: Boundaries of prior β grain size

A line, of length $L_0 = 1$ mm orthogonal to the build direction z , was drawn through each micrograph, and the number of grain boundaries that the line intersects was recorded. The average grain size was calculated by dividing the number of intersections of the line with grain boundaries by the length L_0 of the line. The micrographic evaluations were made using a lateral section of samples (plane x - z).

3.0 RESULTS AND DISCUSSIONS

The numerical results obtained from the tensile tests, density measurements, distortion measurements, and average grain dimension are shown in Table 1, while the trends are represented by colored contour maps in the P - v plane in Figures 5-7.

3.1 Mechanical properties

The mechanical behavior was evaluated through the tensile test in terms of Ultimate Tensile Strength (UTS) (Figure 6a) and Elongation To Failure (ETF) (Figure 6b). Sample ID5 was the one characterized by the highest mechanical resistance, with a UTS of 1156 MPa. The ID7, on the contrary, showed the lowest UTS value equal to 1048 MPa. Overall, for each scan speed value, by increasing the laser power an increase in the mechanical strength was observed until the laser power reached the value of $P = 360$ W (Figure 6a). When the laser power increased to 380 W, a drop in the UTS was observed. It can also be noted how, by increasing the LED, UTS first increased, reaching a maximum when $LED = 0.25$ J/mm, and finally dropped for higher LED values.

This can be explained by looking at the relative density of the samples (Figure 7a), as it will be better detailed in the following. By increasing the laser power, the energy provided to the sample also increased. This has a beneficial effect for specimens produced with lower values of laser power, i.e. from $P = 340$ W to $P = 360$ W, for which the relative

density is around 98.3 %. However, a further increase of the laser power can result in overheating, promoting the formation of gas pores and reducing the density and so the UTS value. A similar trend is reported for the scan speed for a given laser power: increasing the scan speed implies a reduction of the energy provided to the powder, resulting in samples with more porosity. As regards the ETF, the highest value of 9.9% was obtained for ID3, printed with a $P = 380 \text{ W}$ and $v = 1400 \text{ mm/s}$. The ETF results to be strictly correlated to the average size of the prior β -grains and so on the microstructure of the printed sample. Bigger grain size brought higher ductility, as can be observed looking at ID3, characterized by both the highest average grain size and ductility. This statement holds true for scanning speed values less than 1500 mm/s . On the other hand, for $v = 1600 \text{ mm/s}$, an increase in the laser power also leads to higher ETF. This is due to the predominant effect of distortions over the average size of prior β -grains. In opposite to what happened for the UTS, increasing the LED value results in higher ETF. Also, by increasing P and v simultaneously while keeping a constant LED it is possible to obtain samples with better ductility.

Table 1: Ultimate tensile strength (UTS), elongation to failure (ETF), relative density (ρ_r), distortion (Δz), and average grain size obtained for the analyzed samples.

ID	UTS [MPa]	ETF [%]	ρ_r	Δz [mm]	Average prior β grain size [μm]
1	1111±15	7.6±0.2	0.981±0.001	0.965±0.01	97.7±0.6
2	1139±9	8.8±0.3	0.98±0.002	1.1±0.02	99.2±0.5
3	1119±12	9.9±0.1	0.981±0.002	0.93±0.01	102.74±0.6
4	1129±10	7.9±0.1	0.983±0.002	1.21±0.01	98.68±0.2
5	1156±6	8.2±0.4	0.982±0.001	1.23±0.03	100±0.8
6	1123±7	9.1±0.3	0.979±0.001	1.14±0.01	101.35±0.4
7	1048±12	8.4±0.2	0.979±0.001	1.18±0.02	97.6±0.7
8	1126±14	9.3±0.3	0.982±0.002	1.27±0.02	97.9±0.6
9	1119±6	9.5±0.4	0.979±0.002	1.25±0.01	98.04±0.9

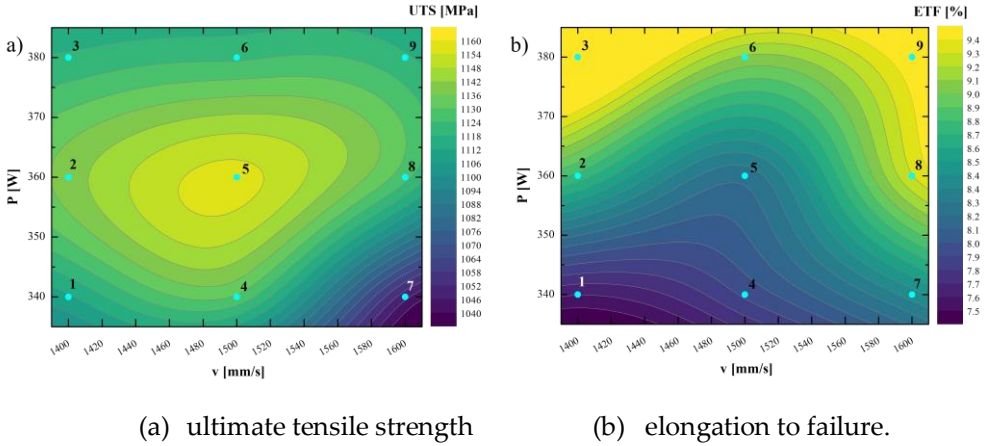


Figure 6. Colored contour maps for parameter trends detection in the P-v plane: (a) ultimate tensile strength, (b) elongation to failure.

3.2 Microstructure

The presence of porosity defects within the sample can lead to a worsening of mechanical properties and material density. It should be pointed out that the chosen range of process parameters results in usable parts with good mechanical properties even if gas pores or lack of fusion defects can be detected [24]. Hence, it can be stated that the range of parameters explored always ensures high relative density values. The trend in relative density, as a function of increasing laser power or scanning speed, as shown in Figure 6a, makes it possible to highlight that the impact of laser scanning speed is limited when the laser power exceeds the 360 W value.

Above the mentioned power value, the relative density remains almost constant as the laser scanning speed changes. Only by varying the laser power it is possible to observe a change in density among the samples. It can be noted that a maximum is reached for the sample ID4, printed with $P = 340$ W and $v = 1500$ mm/s, while, for higher laser power, a drop in density is observed. This can be explained by the progressive formation of gas pores due to higher energy given to the sample. Scan rates higher than 1500 mm/s, for $P = 340$ W, leading to a density reduction due to the activation of lack of fusion defect [9]. Concerning the average grain size of prior β -grains, by increasing the laser power, for fixed scan speed, a higher temperature is reached during the

process allowing the grain to grow. Instead, for higher scan speed the sample is subjected to a faster cooling rate during the process and there is less time for the grains to grow, resulting in samples with smaller grain size (Figure 7b).

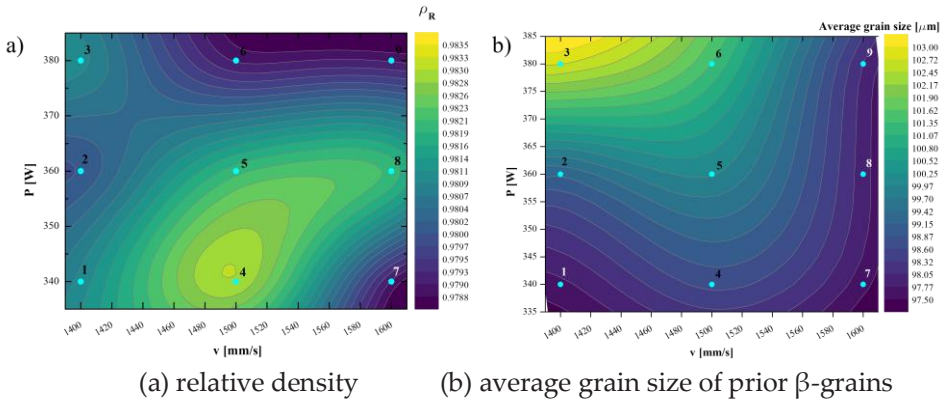


Figure 7. Colored contour maps for parameter trends detection in the P-v plane: (a) relative density; (b) average grain size of prior β -grains.

3.3 Distortions

Distortions are a direct consequence of the residual stress developed during the process in response to high thermal gradients and cooling rates. Increasing the scan speed results in higher cooling rates while increasing laser power leads to a high thermal gradient. It is worth noting that all the specimens showed an upward bending after the removal from the printing plate, and, in this way, it can be stated that a compressive residual state is found in the specimen [25]. In Figure 8 it is possible to see the effect of scan speed on the resulting distortion for samples. Overall, by increasing the scan speed samples with higher distortions are obtained. For scan speed below 1500 mm/s, the lowest distortion values are observed for power equal to 340 W and 380 W.

For each scan speed an increase in laser power results in higher distortion values until $P = 360$ W, while for higher laser power a reduction in distortion can be observed. By increasing the laser power, the higher thermal gradient developed during the process leads to high distortions. For P above 360 W, the power value helps to relax stresses due to deeper remelting of precedent layers [26]. Moreover, the

presence of gas pores acts as stress relief [27, 28].

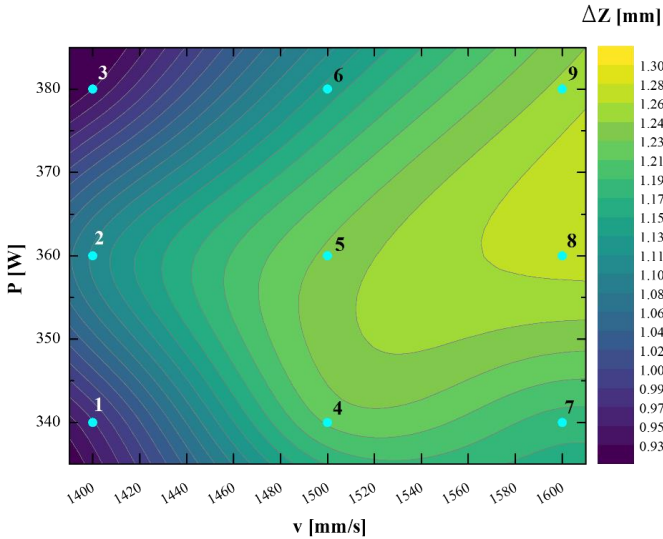


Figure 8. Colored contour maps for parameter trends detection in the P-v plane for distortions in the z-build direction.

3.4 The combined effect of mechanical properties, microstructure, and distortions

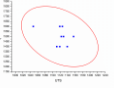
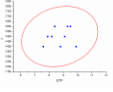
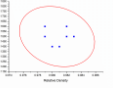
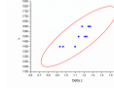
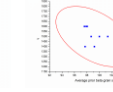
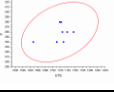
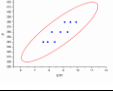
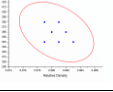
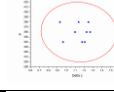
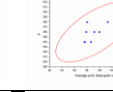
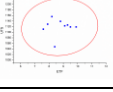
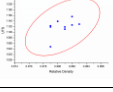
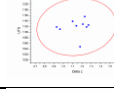
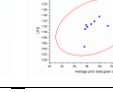
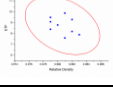
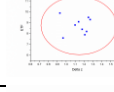
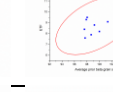
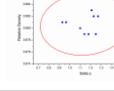
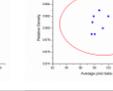
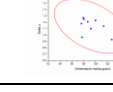
The obtained results showed how UTS and ETF are strictly affected by the microstructural properties, i.e., porosity and average grain size. However, the effect of the distortion and residual stress results is crucial to better understand the trends reported for both UTS and ETF. In detail, residual compressive stress can help improve the resistance of the sample during tensile tests. However, when the laser power increases to 380 W, the detrimental effect of porosity, previously discussed, prevails over the beneficial effect of compressive residual stress.

As regards the ductility of the sample, for scan speed lower than 1500 mm/s the grain size is the most influencing factor, while for higher scan speed the effect of distortion prevails with respect to the grain size dimension. In detail, it can be observed that higher scan speed leads to higher distortion values. The higher the scan speed, the higher the cooling rates, the residual stress, and, as a consequence, the sample distortion. In this way, the high value of ductility measured for high P and v is due to the recovery of the impressed distortion presented in

these samples caused by the building of high residual stress during the printing process.

A scatter plot matrix was generated to emphasize the data correlations. For determining the level of correlation, the Pearson correlation coefficient was calculated. This coefficient measures the entity of the correlation between two variables. The scatter matrix describes a collection of multiple pairwise scatter plots of variables that are presented in a matrix. A positive or negative correlation between the variables can be determined with its help, as well as whether or not the variables are correlated with one another. The scatter plot matrix and the Pearson coefficient are reported in Table 2. The results from this study allow a better understanding of the influence of process parameters on density, microstructure, and distortions on the mechanical properties of Ti-6Al-4V printed parts, their mutual influences, and their correlation.

Table 2: Scatter plot matrix of the experimental data and Pearson correlation index values.

	P	v	UTS	ETF	QR	Δz	Average prior β grain size
P	1	-					
v	-	1					
UTS	-0.37	0.36	1				
ETF	0.17	0.86	0.006	1			
QR	-0.19	-0.38	0.5	-0.35	1		
Δz	0.83	-0.04	0.09	-0.01	0.83	1	
Average prior β grain size	-0.49	0.65	0.35	0.5	-0.01	-0.46	1

4.0 CONCLUSION

In this study, the results of an experimental campaign focused on analyzing the influence of laser power and scan speed on the microstructure, distortions, and mechanical properties of Ti-6Al-4V parts fabricated via L-PBF are shown. Moreover, the combined effect of microstructure, distortions, and mechanical properties of the produced samples has been highlighted. Based on the obtained results, the following main conclusions can be drawn:

- The tensile strength of the sample depends on both laser power and scan speed because of the impact they can have on the measured density and the residual stress state presented within the part.
- The ductility of the samples is affected by both the laser power and scan speed because they have a relevant influence on the resulting microstructure.
- Regarding the microstructure, increasing the laser power leads to a high melt pool temperature, enabling the grain to grow. Increasing the scan speed, instead, results in faster cooling rates and less time for the grains to develop. Thus, producing a smaller grain size.
- Distortions depend on thermal gradients and cooling rates, which are affected by laser power and scan speed, respectively. High laser power and scan speed will result in high residual stress and part distortion.
- The ductility of the sample depends on the measured distortions. By recovering the impressed distortion that was present in these samples, as a result of the occurrence of high residual stress during the printing process, the high value of the ductility measured for samples with high P and v can be explained.
- The porosity within the sample can reduce part distortion. Porosity can have a stress relief effect and a beneficial effect as regards the distortion of the sample due to significant internal free surfaces that allow redistribution of the stresses.

The findings of this study can be utilized as advice by engineers during the design phase to discover the best compromise between part distortion and mechanical qualities for a given application.

AUTHOR CONTRIBUTIONS

G. Pollara - Author: Conceptualization, Data Curation, Methodology, Validation, Software, Writing-Original Draft Preparation, Writing-

Reviewing and Editing; D. Palmeri - Author: Conceptualization, Data Curation, Methodology, Validation, Writing-Original Draft Preparation, Writing-Reviewing and Editing, Supervision;

CONFLICTS OF INTEREST

The manuscript has not been published elsewhere and is not under consideration by other journals. All authors have approved the review, agree with its submission and declare no conflict of interest on the manuscript.

REFERENCES

- [1] T.D. Ngo, A. Kashani, G. Imbalzano, K.T. Nguyen and D. Hui, "Additive manufacturing (3D printing): A review of materials, methods, applications and challenges," *Composites Part B: Engineering*, vol. 143, pp.172-196, 2018.
- [2] M. McGregor, S. Patel, K. Zhang, A. Yu, M. Vlasea, and S. McLachlin, "A Manufacturability Evaluation of Complex Architectures by Laser Powder Bed Fusion Additive Manufacturing," *Journal of Manufacturing Science and Engineering*, vol. 146, no. 6, pp. 1-10, 2024.
- [3] D. Herzog, V. Seyda, E. Wycisk, C Emmelmann, "Additive manufacturing of metals," *Acta Materialia*, vol. 117, pp. 371–392, 2016.
- [4] S. Liu, Y.C. Shin, "Additive manufacturing of Ti6Al4V alloy: A review," *Materials & Design*, vol. 164, pp. 1-23, 2019.
- [5] G. Buffa, D. Palmeri, G. Pollara, F. Di Franco, M. Santamaria & L. Fratini, "Process parameters and surface treatment effects on the mechanical and corrosion resistance properties of Ti6Al4V components produced by laser powder bed fusion", *Progress in Additive Manufacturing*, vol. 9, pp 151–167, 2024.
- [6] P. Mercelis, J.P. Kruth, "Residual stresses in selective laser sintering and selective laser melting," *Rapid Prototyping Journal*, vol. 12, no. 5, pp.254–265, 2006.
- [7] D. Palmeri, G. Pollara, R. Licari, F. Micari, "Finite Element Method in L-PBF of Ti-6Al-4V: Influence of Laser Power and Scan Speed on Residual Stress and Part Distortion," *Metals (Basel)*, vol 13, no. 11, pp. 1-14, 2023.
- [8] T. DebRoy, H.L. Wei, J.S. Zuback, T. Mukherjee, J.W. Elmer, J.O.

- Milewski, A.M. Beese, A.D. Wilson-Heid, A. De and W. Zhang, "Additive manufacturing of metallic components – Process, structure and properties," *Progress in materials science*, vol. 92, pp.112–224, 2018.
- [9] G. Buffa, A. Costa, D. Palmeri, G. Pollara, A. Barcellona, and L. Fratini, "A new control parameter to predict micro-warping-induced job failure in LPBF of Ti6Al4V titanium alloy," *International Journal of Advanced Manufacturing Technology*, vol. 126, no. 3, pp. 1143-1157, 2023.
- [10] H. Shipley, D. McDonnell, M. Culleton, R. Coull, R. Lupoi, G. O'Donnell, and D. Trimble, "Optimisation of process parameters to address fundamental challenges during selective laser melting of Ti-6Al-4V: A review," *International Journal of Machine Tools and Manufacture*, vol. 128, pp. 1–20, 2018.
- [11] L. Mugwagwa, D. Dimitrov, S. Matope, I. Yadroitsev, "Evaluation of the impact of scanning strategies on residual stresses in selective laser melting," *International Journal of Advanced Manufacturing Technology*, vol. 102, pp. 2441–2450, 2019.
- [12] B. Cheng, S. Shrestha, K. Chou, "Stress and deformation evaluations of scanning strategy effect in selective laser melting," *Additive Manufacturing*, vol. 12, pp. 240–251, 2016.
- [13] K. Zeng, D. Pal, C. Teng, B.E. Stucker, "Evaluations of effective thermal conductivity of support structures in selective laser melting," *Additive Manufacturing*, vol. 6, pp. 67–73, 2015.
- [14] T. Yu, M. Li, A. Breaux, M. Atri, S. Obeidat, and C. Ma, "Experimental and numerical study on residual stress and geometric distortion in powder bed fusion process," *Journal of Manufacturing Process*, vol. 46, pp. 214–224, 2019.
- [15] N.C. Levkulich, S.L. Semiatin, J.E. Gockel, J.R. Middendorf, A.T. DeWald and N.W. Klingbeil, "The effect of process parameters on residual stress evolution and distortion in the laser powder bed fusion of Ti-6Al-4V," *Additive Manufacturing*, vol. 28, pp. 475–484, 2019.
- [16] Z. Wang, Z. Xiao, Y. Tse, C. Huang, W. Zhang, "Optimization of processing parameters and establishment of a relationship between microstructure and mechanical properties of SLM titanium alloy," *Optics & Laser Technology*, vol. 112, pp. 159–167, 2019.
- [17] Z. Wang, Z. Xiao, Y. Tse, C. Huang, W. Zhang, "Optimization of processing parameters and establishment of a relationship

- between microstructure and mechanical properties of SLM titanium alloy," *Optics & Laser Technology*, vol. 112, pp. 159–167, 2019.
- [18] J. Liu, Q. Sun, X. Wang, H. Li, K. Guo, J. Sun, "Achieving Ti6Al4V alloys with both high strength and ductility via selective laser melting," *Materials Science and Engineering: A*, vol. 766, pp. 1-8, 2019.
- [19] J. Han, J. Yang, H. Yu, J. Yin, M. Gao, Z. Wang, X. Zeng, "Microstructure and mechanical property of selective laser melted Ti6Al4V dependence on laser energy density," *Rapid Prototyping Journal*, vol. 23, no. 2, pp.217–226, 2017.
- [20] H. Ali, H. Ghadbeigi, K. Mumtaz, "Processing Parameter Effects on Residual Stress and Mechanical Properties of Selective Laser Melted Ti6Al4V," *Journal of Materials Engineering and Performance*, vol. 27, pp. 4059–4068, 2018.
- [21] H. Ali, H. Ghadbeigi, K. Mumtaz, "Effect of scanning strategies on residual stress and mechanical properties of Selective Laser Melted Ti6Al4V," *Materials Science and Engineering: A*, vol. 712, pp. 175–187, 2018.
- [22] A.J. Pinkerton, "Lasers in additive manufacturing," *Optics & Laser Technology*, vol. 78, pp. 25–32, 2016.
- [23] F. Imani, A. Gaikwad, M. Montazeri, P. Rao, H. Yang and E. Reutzel, "Process Mapping and In-Process Monitoring of Porosity in Laser Powder Bed Fusion Using Layerwise Optical Imaging," *Journal of Manufacturing Science and Engineering*, vol. 140, no. 10, pp. 1-14, 2018.
- [24] H Gong, K Rafi, H Gu, T Starr, B Stucker, "Analysis of defect generation in Ti-6Al-4V parts made using powder bed fusion additive manufacturing processes," *Additive Manufacturing*, vol 1, pp. 87–98, 2014.
- [25] C Li, JF Liu, XY Fang, YB Guo, "Efficient predictive model of part distortion and residual stress in selective laser melting," *Additive Manufacturing*, vol. 17, pp. 157–168, 2017.
- [26] L. Mugwagwa, D. Dimitrov, S. Matope, I. Yadroitsev, "Influence of process parameters on residual stress related distortions in selective laser melting," *Procedia Manufacturing*, pp 92–99, 2018.
- [27] P. Bian, J. Shi, Y. Liu, Y. Xie, "Influence of laser power and scanning strategy on residual stress distribution in additively manufactured 316L steel," *Optics & Laser Technology*, vol. 132, p.106477, 2020.
- [28] A.S. Wu, D.W. Brown, M. Kumar, G.F. Gallegos, W.E. King, "An

Experimental Investigation into Additive Manufacturing-Induced Residual Stresses in 316L Stainless Steel,” Metallurgical and Materials Transactions A, vol. 45, pp. 6260–6270, 2014.

